A Parallax-Tolerant Image Stitching Method based on Improved REW

Zhiwei Yin
School of Automation and Information Engineering, Sichuan University of Science and Engineering, Yibin, 644000 China

Xiaogang Wang*
School of Automation and Information Engineering, Sichuan University of Science and Engineering, Yibin, 644000 China

Min Wang
School of Automation and Information Engineering, Sichuan University of Science and Engineering, Yibin, 644000 China

ABSTRACT
Image stitching technology can synthesize multiple images with overlapping areas into a panorama, allowing users to acquire a more complete field of view. However, mainstream image warping methods, when processing images with significant parallax, apply differential deformation operations to pixels on straight-line structures, causing originally straight lines to become bent, broken, or misaligned in the stitched result. This leads to visual distortion, a lack of realism, reduced stitching quality and usability, and amplifies errors in subsequent processing. To address this, this paper proposes a parallax-tolerant image stitching algorithm with straight-line structure preservation. Firstly, the SOLD^2 line detection method is employed to obtain line structures and acquire line endpoints and sample points, providing data for point collinearity constraints and global line construction. Secondly, global lines are constructed using the obtained line structures through parallelism constraints, collinearity constraints, and endpoint distance constraints, providing data for point collinearity constraints to ensure the correct distribution of line structures in the image. Finally, point collinearity constraints based on line endpoints and sample points are added to the REW method to enhance line protection. Experimental results show that the proposed algorithm mitigates the issue of straight-line structure distortion in stitched results from images with large parallax faced by mainstream algorithms. The RMSE on multiple datasets is on average about 0.068 lower than the LPC method and significantly better than other compared algorithms.

General Terms
Computer Vision, Image Processing, Computer Graphics, Algorithms

Keywords
Image Stitching, Parallax, SIFT, REW, Straight-Line Structure Preservation

1. INTRODUCTION
The purpose of image stitching technology is to obtain a wider field of view by constructing different images containing overlapping parts into a panorama with a broader perspective [1]. Currently, image stitching technology has gained extensive attention and application in scenarios such as virtual reality, photogrammetry, aerial map generation, medical image analysis, surveillance video stitching, and 3D reconstruction [2-8]. However, in practical applications, image stitching technology often encounters situations where the camera position moves when capturing the images to be stitched, such as camera translation during UAV aerial photography. This leads to parallax between the acquired images. Mainstream image stitching methods often cause distortion of straight-line structures when stitching images with significant parallax, resulting in poor visual quality of the stitched result or even loss of stitching significance. This makes further research on parallax-tolerant image stitching algorithms with straight-line structure protection highly important.

The AutoStitch algorithm proposed by Brown and Lowe in 2007 is a milestone in the development of image stitching technology. Many subsequent methods have been optimized based on this approach. To date, it remains one of the most widely used stitching algorithms, with mature technology and broad application. However, the stitching quality of such methods significantly degrades when processing images with large parallax. AutoStitch employs the Scale Invariant Feature Transform (SIFT) algorithm summarized and published by Lowe et al. in 2004 to extract feature points, uses feature point matching pairs to calculate image transformation parameters, optimizes these parameters using bundle adjustment, and then applies techniques like illumination compensation and image blending to achieve good stitching results [9]. It is important to note that traditional image stitching methods represented by the AutoStitch algorithm often face challenges when handling large parallax images [10]. Using such methods requires two assumptions: the overlapping regions of the images should ideally lie on the same plane, and the overall scene is best on a single plane; the camera optical centers should nearly coincide during each capture. In practical applications, if parallax exists in the images to be stitched—meaning both factors of different scene depths and different camera optical center positions are present—then because the scene depths differ, multiple planes exist in the scene. If the distance between camera optical centers during capture reaches a certain degree, the relative positions of objects in the images change. The global homography used by such methods cannot align images from multiple planes simultaneously, leading to obvious misalignment and ghosting in the stitched image. This inherent design makes it difficult for such methods to handle images with significant parallax.

Among mainstream methods capable of handling larger parallax, mesh-based stitching algorithms offer good flexibility. Their main idea is to divide the images to be stitched into a mesh grid, treating each grid cell as an independent image for independent warping transformation, greatly increasing the degrees of freedom for warping. Zaragoza et al. proposed the famous As-Projective-As-Possible (APAP) algorithm. It first performs image matching via the SIFT algorithm and calculates a homography matrix, then divides the image into a mesh grid. Using the distance from inliers to the

grid center as weight, combined with the global homography matrix, it calculates a local homography matrix for each grid to guide image warping for stitching [11]. The APAP algorithm achieves high alignment in image overlapping regions with good registration results, becoming a milestone algorithm for subsequent research on mesh optimization methods. However, in such methods, because image transformation is constrained by the grid, image information within a grid cell can transform with the overall grid transformation, but when geometric structures in the image span multiple grid cells, their structural consistency after deformation cannot be guaranteed.

In 2018, He et al. improved the NISwGSP algorithm and proposed the Mesh-based Image Stitching with Line-preservation (MISwLP) algorithm, which reduces straight-line structure distortion to some extent by extracting lines and applying point collinearity constraints. In 2021, Jia et al. proposed the Line-point Consistence (LPC) algorithm, which utilizes point-line consistency to preserve structural information in stitched images under wide parallax conditions and introduced global line structure constraints, addressing the problem of stitching two wide-parallax images [12]. However, both methods struggle to balance straight-line structure protection with local image alignment, potentially causing ghosting or blurring when line protection is good.

Based on this, this paper proposes a parallax-tolerant image stitching algorithm with straight-line structure preservation, aiming to maximally retain the original image structure while maintaining good alignment for parallax images. First, the SOLD2 line detection method [13] is used to acquire line structures, endpoints, and sample points. Second, global lines are constructed using the obtained line structures through parallelism, collinearity, and endpoint distance constraints. Finally, point collinearity constraints based on line endpoints and sample points are added to the REW method [14], and global and local lines are constrained separately to balance line protection and image alignment effects.

2. PROBLEM ANALYSIS

The two key steps in image stitching are registration and blending [15]. Image registration involves selecting a reference image and then using homography transformation to align the overlapping parts of multiple images. Blending synthesizes the registered images into a single image with a wider field of view. Currently, the most common image registration method is feature-point-based matching. Feature-point image matching solves mapping model parameters based on matching relationships between features, capable of overcoming interference from factors like image grayscale, scale, and shooting angle. It is highly reliable, robust, and the mainstream method.

Feature-point-based image registration primarily relies on high-quality feature point matching to form matching pairs, which are then used to calculate the homography matrix for image warping and registration. Mainstream methods, such as the AutoStitch algorithm used in professional stitching software like Image Composite Editor, perform well when stitching texture-rich images. As shown in Figure 1 (left), which are two UAV aerial top-view images of the same playground, the AutoStitch algorithm successfully stitches them. The global homography it uses allows accurate registration due to the small parallax.

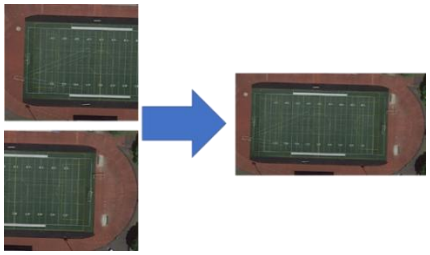

Fig 1: Playground area image stitching

However, the AutoStitch algorithm performs poorly when dealing with images having significant parallax. As shown in Figure 2 (left), which are two images with different scene depths, changed relative object positions due to camera optical center movement, and parallax in the overlapping region, the AutoStitch result shows obvious misalignment. This is because the global homography it uses cannot independently adjust local deformations of the image, thus failing to accurately align multiple objects with changed relative positions and different depths.

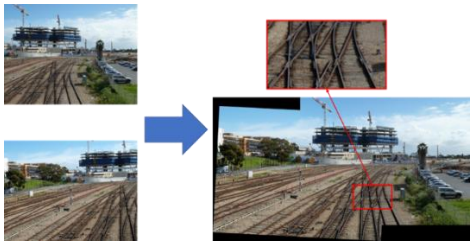

Fig 2: Railway track area image stitching

The current mainstream method for handling larger parallax in image stitching is based on mesh models. By dividing the image into multiple grids, using global homography for pre-registration followed by local homography registration for each grid, this method effectively addresses issues like object misalignment and ghosting in stitching images with significant parallax in overlapping regions. As shown in Figure 3, the mesh-based method eliminates stitching misalignment in the rail track part compared to the global homography method. The mesh deformation and alignment process is shown in Figure 4.

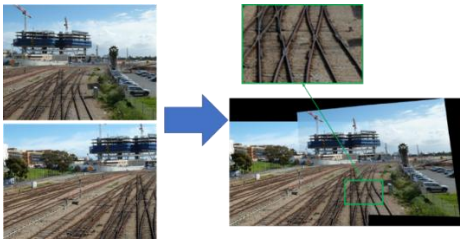

Fig 3: Mesh-based railway track area image stitching

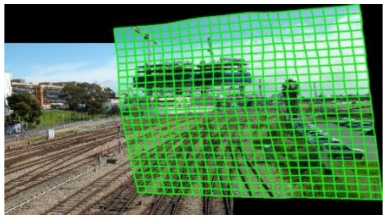

Fig 4: Mesh-based stitching schematic diagram

However, in mesh-based stitching methods, the image to be stitched is transformed constrained by the grid. While image information within a grid cell can transform with the overall grid transformation, geometric structures spanning multiple

grid cells cannot be guaranteed to remain consistent after deformation. Particularly, straight-line structures are prone to breaking or distortion. As shown in Figure 5, the straight-line structure in the stitching result is distorted, such as the horizon line marked in green.

Fig 5: Schematic diagram of straight-line structure distortion

Mainstream global homography methods perform poorly on images with significant parallax in overlapping regions because they cannot align multiple objects with changed relative positions and different depths. Mesh-based stitching methods can eliminate misalignment and ghosting through local deformation but still have geometric structure distortion issues, especially noticeable in straight-line structures. The LPC method uses point-line consistency to preserve structural information in stitched images under wide parallax conditions and introduces global line structure constraints, protecting straight lines in the image. However, it struggles to balance line structure protection with local image alignment, potentially causing ghosting or blurring when line protection is good, as shown in Figure 6 where misalignment and blur occur in the area marked by the red box.

Fig 6: LPC method stitching result

Based on this, this paper proposes a parallax-tolerant image stitching algorithm with straight-line structure preservation, aiming to maximally retain the original image structure while maintaining good alignment for parallax images. First, the SOLD2 line detection method is used to acquire line structures, endpoints, and sample points. Second, global lines are constructed using the obtained line structures through parallelism, collinearity, and endpoint distance constraints. Finally, point collinearity constraints based on line endpoints and sample points are added to the REW method, and global and local lines are constrained separately to balance line protection and image alignment effects.

3. METHOD DESIGN

Based on the above problems, an improved method with straight-line structure protection needs to be designed. First, the SOLD2 method is used to extract line structures. Second, point collinearity constraints are added to the original REW to protect local line structures, while global line segments are constructed and protected to better preserve the overall visual effect of the image. Finally, image alignment and blending with line structure protection are performed. The module structure diagram is shown in Figure 7.

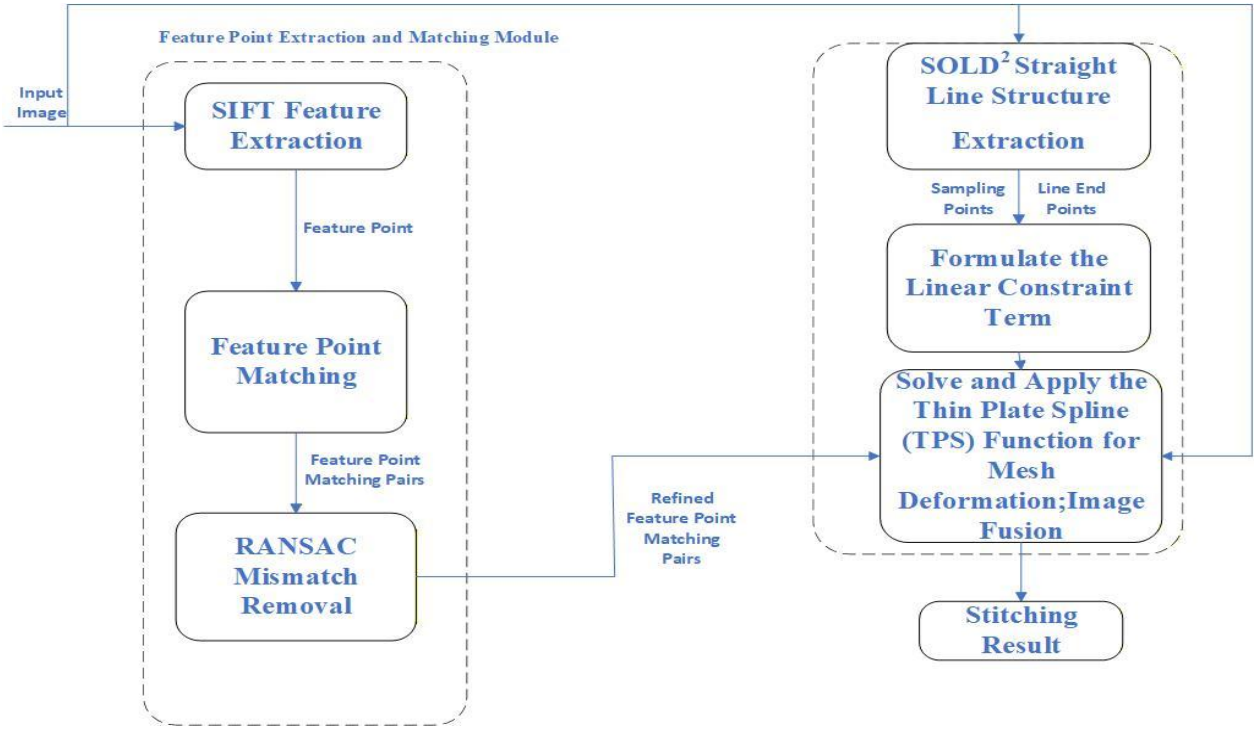

Fig 7: Schematic diagram of the algorithm structure.

3.1 SOLD² Line Detection

The SOLD² line detection method has low dependency on image gradients, adapts to complex scenes, has small localization error, and is robust to occlusion and endpoint variations. Therefore, this method is chosen to acquire image line structures, providing high-quality data for subsequently constructed point collinearity constraints.

SOLD² line segment detection consists of two steps: junction detection and line segment extraction. In the junction detection part, the junction heatmap J^c generated by the network is optimized via a cross-entropy loss over h w/(8×8) . The ground truth junction label $y \in \{1, \dots, 65\}^{\frac{h}{8} \times \frac{w}{8}}$ indicates the junction index in each 8×8 block, with 65 representing no junction. Junction detection is supervised by cross-entropy loss, ensuring the network can accurately classify the junction state of each block. Its loss function is shown in formula (1):

$$\mathscr{L}_{junc} = \frac{64}{h \times w} \sum_{i,j=1}^{\frac{h}{8},\frac{w}{8}} - log\left(\frac{exp(J^c_{ijy_{ij}})}{\sum_{k=1}^{65} \sum^c_{ijk} exp}()\right) \quad (1)$$

During inference, softmax is applied to the channel dimension and the 65th dimension is discarded. Upsampling restores the junction heatmap to size $h \times w$.

In the line heatmap prediction part, the line heatmap H output by the network is optimized via binary cross-entropy loss to minimize the gap between the predicted heatmap H and the ground truth H^{G^T}. H^{G^T} is a binary map where line segment pixels are 1 and non-line pixels are 0. The line heatmap loss function is shown in formula (2):

$$\mathscr{L}_{line} = \frac{1}{h \times w} \sum_{i,j=1}^{h,w} - H^{GT}_{ij}\, log(H_{ij}) \quad (2)$$

Finally, the algorithm extracts line segments from the junction map J and line heatmap H. Thresholding J and applying non-maximum suppression (NMS) yields a junction set $\hat{P}$. All junction pairs form a candidate line segment set $\hat{L}_{\text{cand}}$. For each candidate segment $l_m = (e^1_m, e^2_m)$, regular sampling is conducted, i.e., uniformly sampling Ns = 64 points along the segment; and adaptive local maximum search is performed, i.e., for each sample point q_k, search for the local maximum h_k in the line heatmap within a radius r, where r is proportional to the segment length. The mean heatmap value of the sample points is calculated, a threshold ξ_{avg} = 0.25 is set to filter low-activation segments, and the proportion of points with heatmap values exceeding ξ_{avg}, y_{inlier}, is computed. A threshold ξ_{inlier} = 0.75 is set to ensure segment continuity. The final line segment set $\hat{L}$ consists of candidate segments satisfying the threshold conditions.

3.2 Global Line Segment Construction

First, all line segments in the image $L = \{l_1, l_2, \dots, l_M\}$ are obtained using SOLD² detection. K points $\{p_{j,k}\}_{k=1}^{K}$ are uniformly sampled on each line l_j . Short line segments meeting the conditions are merged into global line segments. Segments to be merged must satisfy three conditions: Parallelism Constraint: The directional angle between the two line segments must be less than a threshold; Collinearity Constraint: The distances from both endpoints of one line segment to the other line segment must be less than a threshold; Endpoint Distance Constraint: The distance between the proximal endpoints of the two segments must be less than a proportional threshold of the distance between the distal endpoints. The algorithm iterates through all line segments, merging qualifying segments based on the above principles to form a global line set S_{gl}. After merging, global lines may span most of the image area, representing long-range structures like building contours or horizons.

3.3 REW Image Warping Method with Added Line Constraints

The REW algorithm achieves good registration on parallax images through mesh-based registration. However, its image registration method does not consider protecting straight-line structures, causing line structures spanning grids to easily distort. Therefore, this paper uses the aforementioned SOLD2 line detection method to obtain the line set, uses the merging operation to obtain the global line set, and constructs point collinearity constraints to protect global and local lines separately, resulting in a stitching algorithm that balances line protection and registration effects.

A line constraint is designed using point collinearity as the criterion, forcing the deformed sample points to be as close as possible to the fitted line l_j^{fit}. The line constraint term is defined as in formula (3):

$$E_l(\hat{V}) = \sum_{j=1}^{M} \sum_{k=1}^{K} \left\| (\tau(p_{j,k}) - \pi_{l_j^{\text{fit}}}(\tau(p_{j,k})) \cdot \mathbf{n}_j \right\|^2 \quad (3)$$

where $\hat{V}$ is the vector of mesh vertex coordinates; M is the number of lines, K is the number of sample points per line; $\tau(p_{j,k})$ is the deformed position of sample point $p_{j,k}$; l_j^{fit} is the optimal line fitted via least squares from the deformed sample points of l_j; $\pi_{l_j^{\text{fit}}}(\cdot)$is the projection operation of a point onto the line l_j^{fit}; $\mathbf{n}_j$ is the unit normal vector of line l_j^{fit}.

For easier optimization, the constraint term can be written in quadratic form, as in formula (4):

$$E_l(\hat{V}) = \left\| W_l \hat{V} \right\|^2 \quad (4)$$

where $\mathbf{W}_l \in \mathbb{R}^{(\sum_{j=1}^{M}(K-1)) \times 2n}$ is the Jacobian matrix, encoding sample point weights and normal vector information, and n is the number of grid vertices.

Since the constraining effects of global and local lines differ, using a larger constraint weight can over-constrain local lines, worsening alignment, while a small weight may insufficiently constrain global lines. Therefore, to further improve line protection, this paper constrains global and local lines separately. The average length of all lines λl is calculated. Lines longer than 3/2 λl are selected as global lines, lines between 3/2 λl and 1/2 λl are local lines, and lines shorter than 1/2 λl are removed as interference. The two types use different weight adjustment parameters. The final line constraint term is as in formula (5):

$$J_L = \mu J_{L_{\text{local}}} + \gamma J_{L_{\text{global}}} \quad (5)$$

where $J_{L_{\text{global}}} = E_{global}$, $J_{L_{local}} = E_{local}$. Parameters μ and γ control the constraint strength for local and global line structures, respectively.

Secondly, the line constraint term J_L is combined with the original REW alignment term J_D and smoothness term J_S to form the total energy function, as in formula (6):

$$J_{\text{total}} = J_D + \lambda J_S + \omega J_L \quad (6)$$

The solution of the energy function J_{total} involves linear system construction and optimization. The original REW linear system is as in formula (7):

$$\begin{pmatrix} \mathbf{K} + \lambda C_{2,2}\mathbf{I} & \mathbf{P} \\ \mathbf{P}^T & \mathbf{0} \end{pmatrix} \begin{pmatrix} \mathbf{w} \\ \mathbf{a} \end{pmatrix} = \begin{pmatrix} \mathbf{f} \\ \mathbf{0} \end{pmatrix} \quad (7)$$

where **K** is the RBF kernel matrix, **P** is the point coordinate matrix, **f** is the bias vector, $C_{2,2}$ is a constant with value 8π. After adding J_L, the system changes to the form in formula (8):

$$\begin{pmatrix} K + \lambda C_{2,2} I + \mu W_L^T W_L & P \\ P^T & 0 \end{pmatrix} \begin{pmatrix} w \\ a \end{pmatrix} = \begin{pmatrix} f \\ 0 \end{pmatrix} \quad (8)$$

where $\mu W_L^T W_L$ is the regularization term for the line constraint.

Since J_L depends on the deformed point positions, direct solution may be nonlinear. Therefore, a two-stage strategy is adopted. The first stage ignores J_L, solving the original REW system to obtain an initial deformation. The second stage calculates $\mathbf{W}_L$ based on the initial deformation, then solves the extended system. Iteration continues until convergence, ensuring the line constraint is effective. The obtained vectors **w** and **a** jointly determine the Thin-Plate Spline (TPS) deformation function. Finally, the TPS function is applied to complete image deformation, alignment, and blending.

4. EXPERIMENTAL RESULTS AND ANALYSIS

The experimental environment for this paper is Ubuntu 18.04 OS, with a 5-core E5-2680 v4 CPU, 27.1GB RAM, RTX 3060 GPU, and 12.6GB VRAM. To verify the effectiveness of the proposed algorithm, stitching experiments were conducted on two sets of images using the proposed algorithm, LPC, and REW respectively. Comparative experiments on stitching accuracy were performed using the proposed algorithm, SVA, CPW, APAP, REW, SPW, and LPC, and the results were uniformly compared and analyzed.

Image stitching experimental results are shown in Figure 8.

(a)

(b)

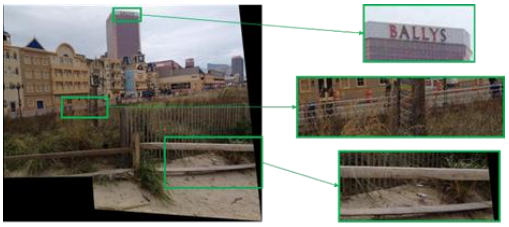

(c)

Figure 8: Algorithm comparison experimental chart.

To quantitatively evaluate algorithm accuracy, Root Mean Square Error (RMSE) is used to assess the positional accuracy of matching points in the overlapping region. The RMSE evaluation formula is defined as follows:

$$\text{RMSE} = \sqrt{\frac{1}{N}\sum_{i=1}^{N}\left(f(p^M i) - p^R{}_i\right)^2} \quad (9)$$

where f represents the grid warping function, N is the number of matching point pairs, $p^M{}_i$ and $P^R{}_i$ are a pair of matching points. A smaller RMSE indicates a better estimated function f and higher point matching accuracy after image transformation.

This paper tested the evaluation metrics for overlapping regions in six scenarios, as shown in Table 1:

From the RMSE data in the table above, the algorithm proposed in this chapter outperforms all compared algorithms. The RMSE value of the proposed algorithm is on average about 0.068 lower than that of the LPC algorithm, and the metrics are significantly better than other compared algorithms. This proves that the proposed algorithm yields smaller registration errors and can effectively improve image stitching quality.

PSNR is a commonly used objective evaluation metric for image quality, representing the ratio of the peak signal power to the power of corrupting noise that affects accuracy. The PSNR evaluation formula is defined as follows:

$$MSE = \frac{1}{m*n}\sum_{i=0}^{m-1}\sum_{j=0}^{n-1}[I_M(i,j) - I_R(i,j)]^2 \quad (10)$$

$$PSNR = 10\,log_{10}\left(\frac{MAX_I^2}{MSE}\right) \quad (11)$$

PSNR is used as a metric to quantitatively evaluate the quality of image fusion. First, the mean squared error (MSE) in the overlapping regions of two registered images is calculated. Then, PSNR is computed based on the maximum pixel value of the images. A higher PSNR value indicates smaller differences between the two images in the overlapping regions, meaning better consistency in the fused content and fewer ghosting or misalignment artifacts. The average PSNR of the method proposed in this paper outperforms other comparative methods, indicating that images fused after registration using the proposed method exhibit less blurring, ghosting, distortion, and other artifacts. The registration performance is superior to other comparative methods, and a comparison of PSNR metrics is shown in the table 2.

Table 1. RMSE Metric Evaluation Values

Dataset/Method	SVA	CPW	APAP	REW	SPW	LPC	Ours
DHW-temple	12.22	2.55	2.04	2.11	2.32	1.76	1.53
APAP-conssite	11.37	7.06	5.13	5.02	4.40	2.03	1.98
APAP-train	9.16	6.34	5.25	4.42	2.11	1.88	1.69
APAP-garden	8.98	6.37	5.19	4.05	2.86	1.44	1.49
DHW-carpark	4.05	3.61	1.38	1.68	1.54	1.32	1.37
SVA-chessgirl	20.78	9.45	2.96	2.78	1.88	1.67	1.63

Table 2. PSNR Metric Evaluation Values

Dataset/Method	SVA	CPW	APAP	REW	SPW	LPC	Ours
DHW-temple	26.32	28.73	29.02	28.86	28.82	30.37	30.62
APAP-conssite	27.07	28.36	28.53	28.96	28.77	28.92	29.67
APAP-train	27.23	28.57	28.38	28.93	28.89	30.02	30.41
APAP-garden	27.77	28.01	28.32	28.52	27.86	30.39	30.51
DHW-carpark	27.95	28.27	29.38	27.71	29.02	29.91	28.85
SVA-chessgirl	26.08	27.44	28.82	28.89	29.33	30.01	30.37

5. CONCLUSION

This paper proposes a new image stitching algorithm. Firstly, the SOLD^2 line detection method is used to obtain line structures, endpoints, and sample points. Secondly, global lines are constructed using the obtained line structures through parallelism, collinearity, and endpoint distance constraints. Finally, point collinearity constraints based on line endpoints and sample points are added to the REW method, and global and local lines are constrained separately to balance line protection effects with image alignment, achieving elastic local registration. Experiments show that the proposed method can better stitch images under large parallax scenes, protect their straight-line structures, and has smaller registration errors. The RMSE value of the proposed algorithm on the datasets is on average about 0.068 lower than that of the LPC algorithm, and the metrics are significantly better than other compared algorithms. Since this study employs traditional handcrafted features, it does not adapt well to weak-texture images. In the future, more adaptive deep learning features suitable for various environments can be considered as a replacement.

6. ACKNOWLEDGMENTS

This work was supported in part by Sichuan Science and Technology Program (No. 2026YFHZ0207), Scientific Research and Innovation Team Program of Sichuan University of Science and Engineering (No. SUSE652A011 , SUSE652B005).

7. REFERENCES

[1] Ghosh, D., & Kaabouch, N. (2016). A survey on image mosaicing techniques. Journal of Visual Communication and Image Representation, 34,1–11.

[2] Wang, J., Wang, C., Chen, W., Dou, Q., & Chi, W. (2024). Embracing the future: The rise of humanoid robots and embodied AI. Intelligent Robotics, 4,196–209.

[3] Chen, X., et al. (2025). Towards intelligent shipping: Image-enhanced ship detection and situation analysis in low-light scenes. Intelligent Robotics, 5(3), 662–678.

[4] Zhang, W., Wang, Y., & Liu, Y. (2022). Generating high-quality panorama by view synthesis based on optical flow estimation. Sensors, 22(2), 470.

[5] Wang, J., Du, P., Yang, S., Zhang, Z., & Ning, J. (2024). A spatial arrangement preservation-based stitching method via geographic coordinates of UAV for farmland remote sensing image. IEEE Transactions on Geoscience and Remote Sensing, 62,1–13.

[6] Lu, T., Li, S., & Fu, W. (2014). Fusion based seamless mosaic for remote sensing images. Sensing and Imaging, 15,101.

[7] Bai, Z., et al. (2020). Real-time video stitching for mine surveillance using a hybrid image registration method. Electronics, 9(9), 1336.

[8] Ha, H. G., Jung, K., Lee, S., et al. (2021). Heterogeneous stitching of X-ray images according to homographic evaluation. Journal of Digital Imaging, 34,1249–1263.

[9] Lowe, D. G. (2004). Sift-the scale invariant feature transform. International Journal of Computer Vision, 2(91-110), 2.

[10] Brown, M., & Lowe, D. G. (2007). Automatic panoramic image stitching using invariant features. International Journal of Computer Vision, 74(1), 59–73.

[11] Huang, J.-B., Kang, S. B., & Ahuja, N. (2013). As-projective-as-possible image stitching with moving DLT. In Proceedings of the IEEE Conference on Computer Vision and Pattern Recognition (CVPR)(pp. 2339–2346).

[12] Jia, Q., Li, Z., Fan, X., Zhao, H., Teng, S., Ye, X., & Latecki, L. J. (2021). Leveraging line-point consistence to preserve structures for wide parallax image stitching. In Proceedings of the IEEE/CVF Conference on Computer Vision and Pattern Recognition (CVPR)(pp. 1–10).

[13] Pautrat, R., Lin, J.-T., Larsson, V., Oswald, M. R., & Pollefeys, M. (2021). SOLD2: Self-supervised occlusion-aware line description and detection. In Proceedings of the IEEE/CVF Conference on Computer Vision and Pattern Recognition (CVPR)(pp. 11368–11378).

[14] Li, J., Wang, Z., Lai, S., et al. (2018). Parallax-tolerant image stitching based on robust elastic warping. IEEE Transactions on Multimedia, 20(7), 1672–1687.

[15] Yang, L., Tian, B., & Dang, J. (2024). Survey on image stitching algorithm based on deep learning. Application Research of Computers, 41(7), 1930–1939.